Imaging of alkyne-functionalized ruthenium complexes for photoactivated chemotherapy

Busemann, A.

2

ALKYNE FUNCTIONALIZATION OF PHOTOACTIVATED RUTHENIUM COMPLEX $[RU(TPY)(BPY)(HMTE)](PF_6)_2$ FOR PROTEIN INTERACTION STUDIES

A synthetic procedure for the generation of the alkyne-functionalized ruthenium polypyridyl complex $[Ru(HCC\text{-}tpy)(bpy)(Hmte)](PF_6)_2$, where HCC-tpy = 4′-ethynyl-2,2′:6′,2′′-terpyridine, bpy = 2,2′-bipyridine, and Hmte = 2-(methylthio)ethanol was developed. The alkyne group allows for the detection of the interaction between the metal complex and bovine serum albumin (BSA) using copper-catalyzed click chemistry with an azide-labelled fluorophore and gel electrophoresis. This method demonstrates that a) the interaction between the ruthenium complex and BSA is strictly controlled by light irradiation and b) visualization is possible of weak complex-protein interactions that are difficult to study using traditional methods such as UV-vis spectroscopy or ESI MS. Overall, these results indicate that the combination of photoactivation and fluorophore post-labelling is an elegant method to study weak interactions.

2.1 Introduction

Cytotoxicity assays, cell uptake studies, and cell fractionation experiments are typically performed to study the biological effects and the intracellular fate of metal-based anticancer compounds.[1-4] In addition, experiments regarding the interaction of the metallodrug with isolated biomolecules provide insights about possible targets and binding sites. A frequently studied protein in bioinorganic chemistry is serum albumin. It is the most abundant protein in the blood stream (35 − 50 g/L) and thus a highly likely binding partner for injected metallodrugs. Serum albumin is responsible for the transport of biomolecules,[5] it can act as drug carrier and reservoir,[6-10] and might support drug accumulation in tumor cells.[6] It has, however, been demonstrated that interaction of anticancer drugs with serum albumin can cause undesired side effects,[6, 11] and can hinder the interaction with the actual targets of the drug.[12] Bovine serum albumin (BSA) is a model protein for human serum albumin (HSA),[10] with which it shares 76% of sequence homology,[13] and it is a major component of cell-growth medium.

Common methods to investigate metallodrug-protein interactions are X-ray diffraction analysis,[11, 14, 15] electrospray ionization mass spectrometry (ESI),[16] UV-vis spectroscopy,[17] and circular dichroism (CD) spectroscopy.[18] For emissive metallodrugs, the complex and its interaction with biomolecules can be imaged in gel electrophoresis or in cells by emission microscopy.[19, 20] An effective approach to visualize non-emissive complexes is fluorophore labeling of the metallodrug *via* Cu(I)-catalyzed azide-alkyne cycloaddition (CuAAC).[21, 22] However, this method requires the modification of the complex with an azide or alkyne click handle. The synthesis of those functionalized polypyridyl complexes is challenging: Azide-functionalized ruthenium complexes are known to be unstable,[23, 24] and alkynes can act as ligands for ruthenium and cobalt centers,[25] leading to formation of byproducts.[26] So far, higher yields for the synthesis of alkyne-functionalized ruthenium complexes are only achieved by utilization of silver(I) ions. These are used to either enhance the ligand exchange process,[23] or to remove the protecting group that was used to prevent alkyne coordination to the metal center.[27] Silver ions, however, are toxic and thus, the complexes synthesized according to these reaction procedures may contain traces of the heavy metal and thus cannot be used in living systems.[28]

The ruthenium polypyridyl complex [Ru(tpy)(bpy)(Hmte)]$(PF_6)_2$ ([**1**]$(PF_6)_2$, where tpy = 2,2′:6′,2″-terpyridine, bpy = 2,2′-bipyridine, and Hmte = 2-(methylthio)ethanol) is such a non-emissive complex that cannot be easily followed in cells.[29] In the dark, the interaction of [**1**]$(PF_6)_2$ with proteins is prevented by the protecting monodentate Hmte ligand. Only after controlled photosubstitution of the thioether ligand by a solvent molecule, coordination of the activated drug to proteins or DNA is possible, an idea that is central in ruthenium-based photoactivated chemotherapy (PACT).[30, 31] By doing so, the biological activity of the metal complex can be controlled, in contrast to thermally unstable complexes such as [Ru(tpy)(bpy)(Cl)]Cl or RAPTA-C, which hydrolyze quickly in aqueous solution.[32-34] However, this light-controlled protein interaction has never been demonstrated experimentally. Here, an alkyne-functionalized analogue of photoactivatable ruthenium complex [**1**]$(PF_6)_2$ was synthesized, [Ru(HCC-tpy)(bpy)(Hmte)]$(PF_6)_2$ ([**2**]$(PF_6)_2$, where HCC-tpy = 4′-ethynyl-2,2′:6′,2″-terpyridine). The synthesis procedure of the complex with a simple CCH group was developed, and the light-controlled interaction of [**2**]$(PF_6)_2$ with BSA was studied by fluorophore labeling *via* CuAAC (Scheme 2.1). This method is compared with two known methods for studying BSA-metallodrug interaction, *i.e.* UV-vis spectroscopy and ESI MS.

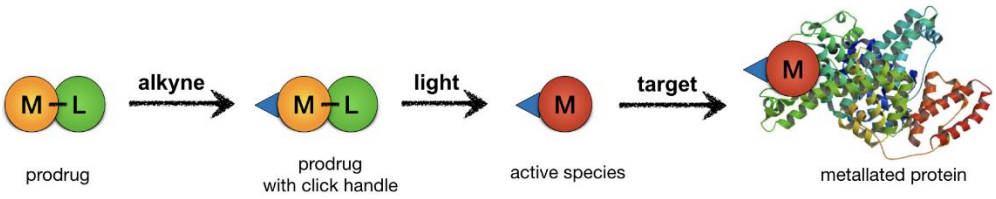

Scheme 2.1. Schematic overview of the interaction of an alkyne-functionalized ruthenium-based drug with its biological target after visible light activation.

2.2 Results and Discussion

2.2.1 Synthesis and characterization

An alkyne-functionalized analogue of the ruthenium polypyridyl complex [**1**]$(PF_6)_2$ was synthesized by placing an alkyne moiety in the 4′-position of the tpy ligand. By doing so, the symmetry of the resulting complex is preserved, while monosubstitution of the ligands on any other position would lead to the formation of stereoisomers. Since the alkyne-protecting triisopropylsilyl (TIPS) group was reported to be difficult to remove,[35] the use of trimethylsilyl (TMS) and *tert*-butyldimethylsilyl (TBDMS) was investigated. Both are known protecting

groups for terminal alkynes, but they are more readily removed compared to TIPS. In our hands, the TMS protecting group was not stable enough to withstand subsequent reaction steps, leading to the formation of undesired byproducts. Therefore, the synthesis of the alkyne-functionalized ruthenium complex [**2**]$(PF_6)_2$ was finally realized using the TBDMS group (Scheme 2.2). The alkyne-functionalized tpy ligand (RCC-tpy, where R = TBDMS) was synthesized using a Sonogashira coupling,[26] purified by column chromatography, and the desired product RCC-tpy was obtained with a yield of 95%. Instead of using a ruthenium(II) precursor, as reported elsewhere,[27, 36] RCC-tpy was reacted with ruthenium(III) chloride, to obtain [Ru(RCC-tpy)$(Cl)_3$] ([**3**]). The reaction with bpy in ethanol/water (3:1) yielded the desired ruthenium(II) product [Ru(RCC-tpy)(bpy)(Cl)]Cl ([**4**]Cl) in a yield of 83%. The chloride ligand was then substituted in a reaction with Hmte in pure water at 60 °C for 16 h. Precipitation of the product after the reaction was achieved by addition of saturated aqueous potassium hexafluoridophosphate. Two singlets at 1.10 and 0.32 ppm in the ^{1}H NMR spectrum in acetone-d_6 (Figure AII.1) integrating for nine and six protons, respectively, and the major peak in the MS spectrum at m/z = 360.9 confirmed the stability of the TBDMS protecting group during ligand exchange and the nature of [Ru(RCC-tpy)(bpy)(Hmte)]$^{2+}$ (calc. m/z = 360.6 for [**5**]$^{2+}$). Noteworthy, when coordination of Hmte was performed at 80 °C, TBDMS protection was not fully retained, resulting in the formation of byproducts. Analysis of these byproducts showed that the ruthenium center can act as a catalyst in the reaction of a terminal alkyne with alcohol groups (ethanol or Hmte), leading to formation of enol esters (see Scheme AII.1).[37] These findings emphasized that the TBDMS protecting group was necessary to protect the alkyne as long as the ruthenium center bears labile ligands or goes through ligand exchange. Controlled deprotection of the alkyne in [**5**]$(PF_6)_2$ was performed using five equivalents of potassium fluoride in methanol at 30 °C. ^{1}H NMR in acetone-d_6 shows the disappearance of the two singlets of the protecting TBDMS group concomitant with the appearance of a new singlet at 4.55 ppm integrating for one proton, characteristic for the free alkyne (Figure AII.2). In combination with mass spectrometry, the successful synthesis of [Ru(HCC-tpy)(bpy)(Hmte)]$(PF_6)_2$ ([**2**]$(PF_6)_2$, m/z = 303.5; calc. m/z = 303.6 for [**2**]$^{2+}$), was confirmed.

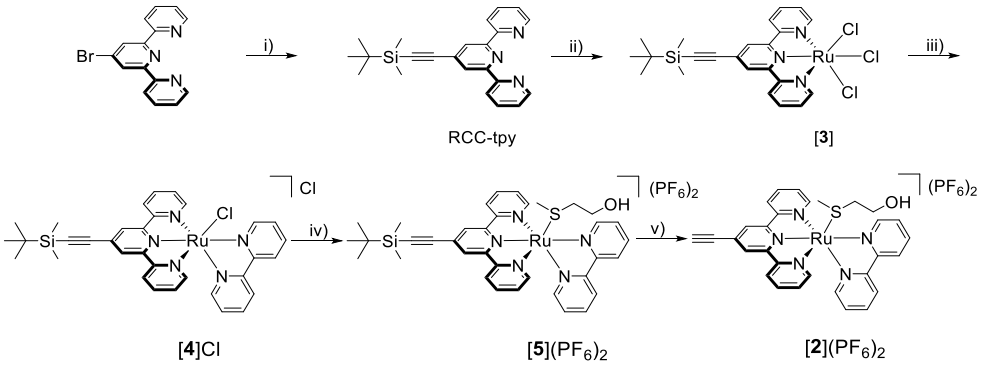

Scheme 2.2. Reaction scheme of the stepwise synthesis of [**2**](PF$_6$)$_2$. Conditions: i) CuI, Pd(PPh$_3$)$_2$Cl$_2$, TBDMS-ethyne, Et$_3$N, 80 °C, N$_2$, 7 h; 95% ii) RuCl$_3$, ethanol, 80 °C, 16 h; 75% iii) bpy, LiCl, Et$_3$N, ethanol/water (3:1), 60 °C, 16 h; 83% (iv) Hmte, water, 60 °C, N$_2$, 16 h, aq. KPF$_6$; 85% v) KF, methanol, 30 °C, 16 h, aq. KPF$_6$; 76%.

Dark red rhombic single crystals of [**2**](PF$_6$)$_2$ suitable for X-ray structure determination were obtained through slow vapor diffusion of diisopropyl ether into a solution of [**2**](PF$_6$)$_2$ in acetonitrile (Figure 2.1). Selected bond lengths and angles are summarized in Table 2.1, together with those reported for the structure of [**1**](PF$_6$)$_2$.[29] The alkyne bond length (C17≡C16 = 1.180(4) Å) is comparable with that of published data.[27] The Ru-N bond distances of the tpy as well as of the bpy ligand in [**2**](PF$_6$)$_2$ are not significant different from those in the non-functionalized analogue [**1**](PF$_6$)$_2$. Hmte is bound *via* the sulfur atom with a Ru-S bond distance of 2.3764(6) Å, which is slightly longer than in [**1**](PF$_6$)$_2$.[38] Therefore, it can be concluded that the alkyne moiety has no significant effect on the geometry of [**2**](PF$_6$)$_2$ compared to [**1**](PF$_6$)$_2$.

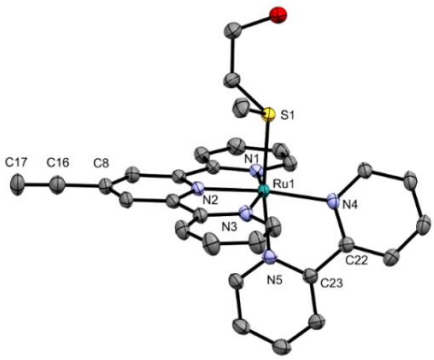

Figure 2.1. Displacement ellipsoid (50% probability level) of the cationic part of [**2**](PF$_6$)$_2$ as observed in the crystal structure. Counter ions and H atoms have been omitted for clarity.

Table 2.1. Selected bond lengths (Å) and angles (°) for [**2**](PF$_6$)$_2$ and [**1**](PF$_6$)$_2$.

	[**2**](PF$_6$)$_2$	[**1**](PF$_6$)$_2$ [a]
Ru-N1	2.0566(19)	2.061(1)
Ru-N2	1.9568(19)	1.961(1)
Ru-N3	2.0709(19)	2.066(1)
Ru-N4	2.0948(18)	2.092(1)
Ru-N5	2.0676(19)	2.064(1)
Ru-S1	2.3764(6)	2.3690(5)
C17-C16	1.180(4)	-
C16-C8	1.440(3)	-
N1-Ru1-N2	79.90(8)	80.08(6)
N2-Ru1-N3	79.92(8)	79.39(6)
N1-Ru1-N3	159.55(8)	159.31(6)
N4-Ru1-N5	78.12(7)	78.12(6)

[a] Data taken from Bahreman *et al*.[29]

2.2.2 Photochemistry of [2](PF$_6$)$_2$

[**1**](PF$_6$)$_2$ is known to be stable in the dark while light irradiation initiates the substitution of the thioether ligand by a water molecule ([**6**]$^{2+}$, Scheme 2.3).[29] To test whether alkyne-functionalized [**2**](PF$_6$)$_2$ possesses the same photochemical properties, UV-vis spectra of a solution of [**2**](PF$_6$)$_2$ in water were recorded. The absorbance spectrum of [**2**](PF$_6$)$_2$ in aqueous solution is characterized by an absorption maximum at 470 nm, and when kept in the dark, the complex is stable at 37 °C for 16 h (see Figure AII.3 and AII.4). However, when irradiated with a green LED (517 nm) at 37 °C in water, the UV-vis spectrum of [**2**](PF$_6$)$_2$ showed a bathochromic shift of the maximum to 491 nm (Figure 2.2). This change was accompanied by a change of the major peaks in MS spectra from m/z = 303.2 ([**2**]$^{2+}$, calc. m/z = 303.6) to m/z = 266.2, indicating the formation of the aqua complex [Ru(HCC-tpy)(bpy)(OH$_2$)]$^{2+}$ ([**7**]$^{2+}$, calc. m/z = 266.5, Figure AII.5). The photosubstitution was completed after approximately 30 min of irradiation, corresponding to a photosubstitution quantum yield Φ_{470} of 0.021 in water (Table 2.2). These results are comparable to those found for the non-functionalized analogue [**1**](PF$_6$)$_2$, which under blue light irradiation (452 nm) showed a quantum yield Φ_{450} of 0.022.[29] In addition, [**1**](PF$_6$)$_2$ and [**2**](PF$_6$)$_2$ show similar low singlet oxygen generation quantum yields (Φ_Δ) and phosphorescence quantum yields (Φ_P)

(Table 2.2, Figure AII.6). These results demonstrated that the alkyne moiety in $[\mathbf{2}]^{2+}$ does not have a significant effect on the photochemical properties of the complex compared to $[\mathbf{1}]^{2+}$.

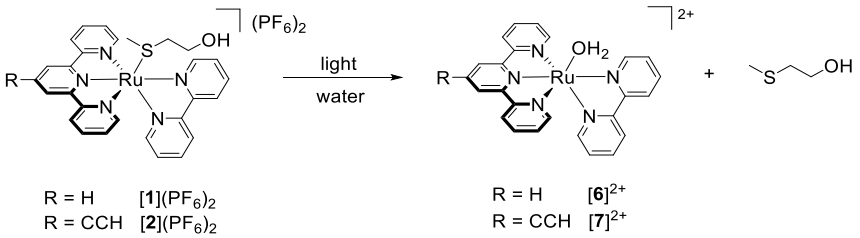

Scheme 2.3. Photosubstitution reaction of $[\mathbf{1}](PF_6)_2$ and $[\mathbf{2}](PF_6)_2$ in aqueous solution.

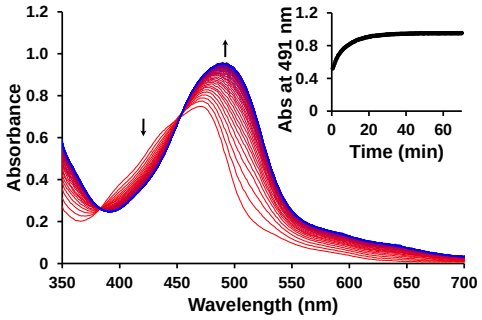

Figure 2.2. Evolution of the UV-vis absorption spectra (region 350 – 700 nm) of a solution of $[\mathbf{2}](PF_6)_2$ in water upon green light irradiation. Conditions: [Ru] = 0.074 mM, T = 37 °C, light source: λ = 517 nm, $\Delta\lambda_{1/2}$ = 23 nm, 5.42 mW, photon flux $\Phi = 5.4 \cdot 10^{-8}$ mol · s^{-1}, V = 3 mL, under air atmosphere. Inset: Time evolution of absorbance at wavelength 491 nm.

Table 2.2 Maximum absorption wavelengths (λ_{max} in nm), molar absorption coefficient (ε in M^{-1} · cm^{-1}), phosphorescence quantum yield (Φ_P) in methanol-d$_6$, singlet oxygen generation quantum yield ($\mathbf{\Phi_\Delta}$) in methanol-d$_6$, and photosubstitution quantum yields (Φ_{max}) in water at 25 °C for complexes $[\mathbf{2}](PF_6)_2$ and $[\mathbf{1}](PF_6)_2$.

	$\boldsymbol{\lambda_{max}}$ [a]	$\boldsymbol{\varepsilon_{\lambda max}}$ [a]	$\mathbf{\Phi_P}$ [b]	$\mathbf{\Phi_\Delta}$ [b]	$\mathbf{\Phi_{max}}$ [a]
$[\mathbf{2}](PF_6)_2$	470	$9.54 \cdot 10^3$	$< 1.0 \cdot 10^{-4}$	0.007	0.021 [d]
$[\mathbf{1}](PF_6)_2$	450 [c]	$6.60 \cdot 10^3$ [c]	$< 1.0 \cdot 10^{-4}$	< 0.005	0.022 [c, e]

[a] in MiliQ water, [b] in methanol-d$_6$, [c] Data from Bahreman *et al.*[29], [d] at 470 nm, [e] at 450 nm

2.2.3 CuAAC reaction on ruthenium complex

To test whether the alkyne-functionalization allows for the CuAAC reaction on the ruthenium complex, $[\mathbf{2}](PF_6)_2$ was reacted with an excess of 2-(2-(2-azidoethoxy)ethoxy)ethanol in the presence of catalytic amounts of Cu(II)

and sodium ascorbate in a water/acetone mixture (9:1) at 25 °C for 1 h (Scheme 2.4). MS analysis of the reaction mixture showed peaks centered at m/z = 391.2 corresponding to the click product $[\mathbf{8}]^{2+}$ (calc. m/z = 391.1). The signal of the starting material $[\mathbf{2}]^{2+}$ at calc. m/z = 303.6 had disappeared. After liquid-liquid extraction from dichloromethane, the ^{1}H NMR spectrum in acetone-d_6 showed no singlet peak at 4.56 ppm corresponding to the terminal alkyne, but a new singlet at 9.04 ppm for the triazole formation (Figure AII.7). Overall, the CuAAC reaction on $[\mathbf{2}](PF_6)_2$ was successful and full conversion after 1 h reaction time was demonstrated.

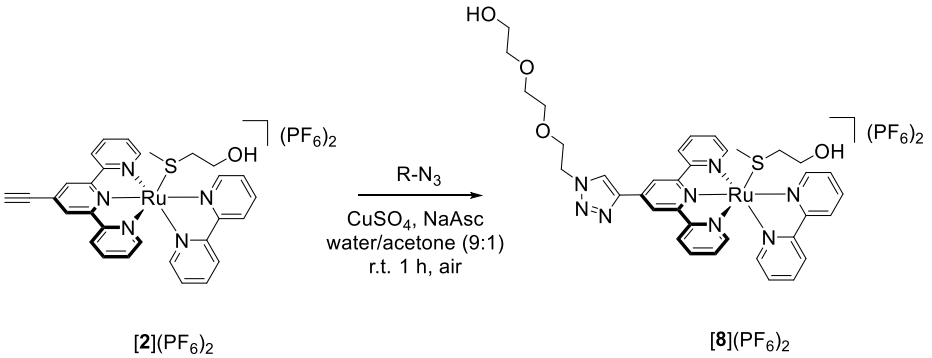

Scheme 2.4. Reaction procedure of the CuAAC reaction of $[\mathbf{2}](PF_6)_2$ with R-N_3 (2-(2-(2-azidoethoxy)ethoxy)ethanol).

2.2.4 Investigation of the interaction between $[2]^{2+}$ and BSA

The interaction of $[\mathbf{2}](PF_6)_2$ and BSA was investigated by fluorophore-labeling *via* CuAAC reaction on the alkyne-functionalized complex-BSA adduct with an azide-fluorophore (Alexa Fluor™ 647 azide, A647), and analyzed by gel electrophoresis (Figure 2.3). Incubation of Hmte-protected $[\mathbf{2}](PF_6)_2$ (75 μM) with BSA (15 μM) for 24 h at 37 °C in the dark did not result in a fluorescent signal after the CuAAC reaction (Figure 2.3, lane 1), indicating that the protected complex could not bind to BSA. However, when the mixture was irradiated with green light (λ = 520 nm) for 1 h, and then further incubated with BSA in the dark for 6 or 24 h, a fluorescent band appeared between 55 and 70 kDa (Figure 2.3, lane 6 for 6 h and lane 12 for 24 h). This result indicated that i) light-activation of the complex was successful and allowed for controlling the interaction of the complex with BSA, ii) the complex-BSA adduct can be labelled with a fluorophore by CuAAC, and iii) adduct formation between the ruthenium complex and BSA increases over time (quantitatively shown by elevated levels of fluorescence intensity of the band when going from 6 to 24 h incubation time). Several negative controls were performed *e.g.* samples with non-functionalized complex $[\mathbf{1}](PF_6)_2$ (Figure 2.3, lane 3 and 8) or without any complex (Figure 2.3, lane 5). These samples did not result in any

significant labelling. A low background fluorescence in lane 5 was observed due to unspecific binding of the fluorophore A647 to BSA. Indeed, this was confirmed by BSA-free controls (lane 4) and fluorophore-free controls (lane 2, 7, and 10 in Figure 2.3), as these did not exhibit any fluorescence. If not activated, [**2**](PF$_6$)$_2$ remained thermally stable for the entire incubation time (lane 13 in Figure 2.3 and Figure AII.4). Upon increased BSA concentrations, the intensity of the fluorescent band increased as well (BSA concentrations vary from 5 to 20 μM, Ru:BSA 5:1, 5:3, and 5:5, Figure AII.8 and AII.9). These experiments showed that the fluorescence intensity of the bands is correlated to the increased BSA concentration. Thus, the interaction between [**2**]$^{2+}$ and BSA appears to be dose-dependent.

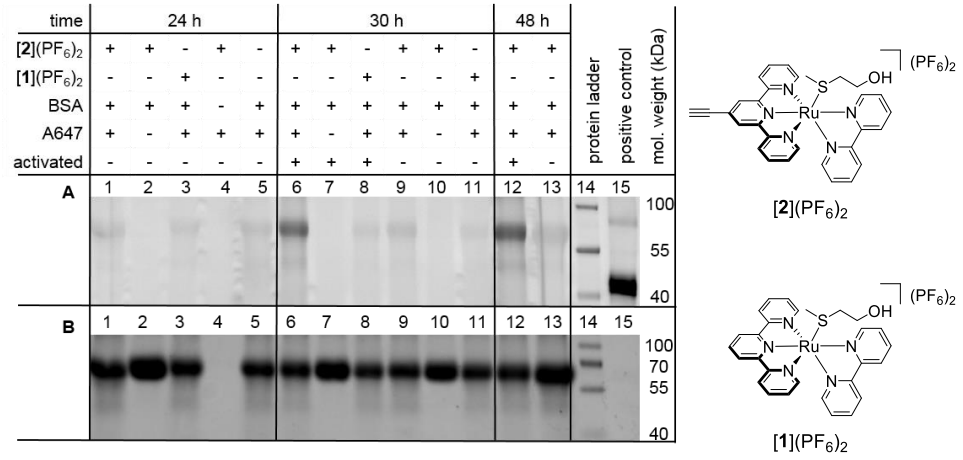

Figure 2.3. Polyacrylamide gel electrophoresis (PAGE) showing post-labeled Ru-bound BSA (A). Fluorescence labeling is achieved *via* CuAAC reaction with A647. The protecting Hmte ligand of [**2**](PF$_6$)$_2$ prevents interaction with BSA, resulting in the absence of fluorescence labeling (lane 1, 9, and 13). Light irradiation after 24 h generates the aqua complex [**7**]$^{2+}$ that interacts with BSA after 6 and 24 h incubation in the dark (lane 6 and 12, respectively). Control reactions with alkyne-free [**1**](PF$_6$)$_2$ (lane 3 and 8), without A647 (lane 2, 7, and 10), and without BSA (lane 4) show no fluorescent labeling. Coomassie staining (B). Conditions: [Ru] = 75 μM, [BSA] = 15 μM. Green light activation: λ = 520 nm, light dosage: 76 J/cm^2, t = 1 h, T = 37 °C. Click conditions: 2.5 μM A647, 3.2 mM $CuSO_4$, 18.8 mM NaAsc, 0.7 mM THPTA, 46.3 mM Tris-HCl, t = 1h, T = 25 °C. Lane 14: prestained protein ladder, lane 15: positive control: alkyne-substituted vinculin, Homopropargylglycine-Vin.

To further explore the added value of this method to study the BSA-Ru interaction, the interaction between the ruthenium complex and BSA was investigated with UV-vis spectroscopy. First, the absorbance spectra of solutions of only the complexes (15 μM) or BSA (15 μM) were recorded separately in PBS for 24 h at 37 °C (Figure AII.10 and AII.11). The unchanged UV-vis spectra indicated the thermal stability of

both individual species. Thereafter, the absorbance spectra of mixtures of the ruthenium complexes (15 μM) and BSA (15 μM) were recorded under the same conditions. The spectrum of the solution of [**1**](PF$_6$)$_2$ and BSA did not change during 24 h, as expected for the Hmte-protected complex (Figure 2.4a). However, when using [**6**]$^{2+}$, the UV-vis spectrum also did not show a change (Figure 2.4b). Similar results were obtained when using alkyne-functionalized complexes [**2**](PF$_6$)$_2$ and [**7**]$^{2+}$ in the presence of BSA (Figure 2.4c and d). Therefore, it appeared that the interaction between ruthenium complexes and BSA after light activation cannot be monitored using UV-vis spectroscopy under the conditions reported.

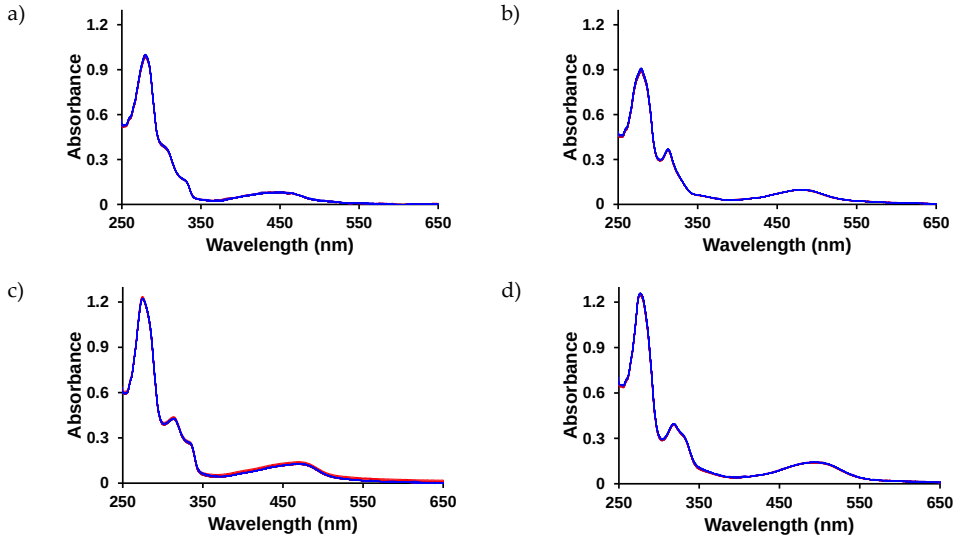

Figure 2.4. Evolution of the UV-vis spectra (region 250 – 650 nm) of a solution of ruthenium complex (0.015 mM) with BSA (0.015 mM) in PBS under air atmosphere for 24 h at 37 °C. a) [**1**](PF$_6$)$_2$, b) [**6**]$^{2+}$, c) [**2**](PF$_6$)$_2$, d) [**7**]$^{2+}$.

Mass spectrometry is also a very powerful method to study protein-metallodrug interactions.[39-41] ESI MS spectra were recorded to quantify the amount of ruthenium complexes interacting with BSA. Different mixtures of [**1**](PF$_6$)$_2$ (100, 300, or 500 μM) and BSA (100 μM) in aqueous solution were incubated at 37 °C for 24 h in the dark and were activated thereafter with green light (517 nm) for 1 h. 24 h After light activation, samples were subjected to ESI-MS analysis. The presence of the activated ruthenium species led to a signal broadening and loss of spectral resolution compared to BSA only (66429 Da). However, no evident signals that can be ascribed to Ru-BSA adducts were detected. To improve the signal, ultrafiltration with a 10 kDa cut-off was performed, followed by extensive washing steps. Upon this

treatment, spectra showed a better resolution, but the signal showed only unreacted BSA. Analysis of the ultrafiltered fraction by ICP-AES revealed that indeed very little ruthenium was present in the BSA samples (see Table AII.1). These results suggest that the interaction between the ruthenium species and BSA is of non-covalent nature and too weak to be detected by mass spectrometry after ultrafiltration. Control experiments with [**2**]$(PF_6)_2$ were performed and resulted in similar spectra, indicating that the alkyne-functionalization did not cause an enhanced interaction of the ruthenium center with BSA.

Fluorescent labeling clearly showed that the activated ruthenium complex interacts with BSA, and that this interaction is concentration dependent. On the other hand, the results from ESI MS and UV-vis spectroscopy suggest that the binding is weak, since no signal of a ruthenated protein was observed after sample preparation. Strong covalent binding of the ruthenium complex to methionine and histidine residues, as seen with other ruthenium complexes,[17, 32, 42-45] can therefore be excluded. In addition, BSA contains 35 cysteine residues, forming 17 disulfide bridges. Therefore, only one thiol group is available for binding, Cys34.[46] However, the bond between cysteine and ruthenium(II) is oxygen-sensitive. Once coordinated to ruthenium, cysteine is easily oxidized, which leads to the formation of unstable sulfenato and sulfinato ruthenium complexes, that ultimately release the hydrolyzed ruthenium complexes [**6**]$^{2+}$ and [**7**]$^{2+}$.[47] Another possibility is that the activated ruthenium complex might interact non-covalently with the hydrophobic core of BSA, similar to what has been described for KP1019 with HSA.[48, 49] Therefore, it is reasonable to hypothesize that the weak interaction between the aqua complexes and BSA occurs either *via* coordination to Cys34 followed by oxidation, or *via* non-covalent interactions with the hydrophobic pockets of BSA. Since in gel fluorescence showed that the intensity of the fluorescent band corresponding to the ruthenated BSA increased with incubation time, the interaction *via* Cys34 coordination can be excluded due to its instability over time. Overall, our data indicate that after light activation the corresponding aqua complex interacts non-covalently with BSA *via* weak interactions, rather than *via* coordination to Cys34 or other protein residues.

2.3 Conclusion

To conclude, a synthetic route was developed for the functionalization of a photolabile ruthenium complex with an alkyne handle. The TBDMS group appears

to be the best alkyne protecting group during ligand introduction and exchange, preventing the formation of side products. In addition, this protecting group is easily removed with a small excess of potassium fluoride, without the need for toxic silver ions. The small alkyne handle allowed for fluorophore post-labeling *via* CuAAC to study the non-covalent interactions between the ruthenium complex and BSA, which were very difficult to detect with state-of-art methods such as UV-vis spectroscopy and mass spectrometry. In addition, fluorophore post-labeling also demonstrate the protective character of the thioether ligand regarding the interaction of [**1**]$^{2+}$ or [**2**]$^{2+}$ with the protein, which lies at the core of photoactivated chemotherapy. As an interaction between the metal complex and BSA was only detected after light activation, it can be hypothesized that PACT prodrugs have little interaction with blood proteins before light activation, which may result in poor systemic toxicity, compared to drugs that activate spontaneously by thermal hydrolysis or reduction. Overall, fluorophore labeling *via* CuAAC on alkyne-functionalized prodrugs appears to be an excellent way to visualize even weak interactions between metallodrugs and proteins.

2.4 Experimental

2.4.1 Materials and Methods

4′-Bromo-2,2′:6′,2″-terpyridine and 2,2′-bipyridine were purchased from TCI Europe, $RuCl_3$ from Alfa Aesar, 2-(methylthio)ethanol, and *tert*-butyldimethylsilylethyne from Sigma Aldrich. [**1**]$(PF_6)_2$ was synthesized according to literature.[29] All metal complexes were synthesized in dim light and stored in darkness. All commercial reactants and solvents were used without further purification. ^{1}H NMR spectra were recorded on a Bruker AV-300 spectrometer. Chemical shifts are indicated in ppm. Mass spectra were recorded by using an MSQ Plus Spectrometer.

2.4.2 Synthesis

RCC-tpy (R = TBDMS)

RCC-tpy was synthesized using an adapted literature procedure.[26] To dry and degassed triethylamine (12 mL), 4′-bromo-2,2′:6′,2″-terpyridine (1.0 g, 3.2 mmol), copper(I) iodide (38 mg, 0.20 mmol), dichlorobis(triphenylphosphine)palladium (70 mg, 0.10 mmol), and *tert*-butyldimethylsilylethyne (1.0 mL, 5.3 mmol) were added under dinitrogen atmosphere. The reaction mixture was stirred and refluxed for 7 h at 80 °C under dinitrogen atmosphere. During reflux the same amounts of triethylamine and *tert*-butyldimethylsilylethyne were added twice (after 2 h 20 min and 4 h 40 min). The solvent was evaporated with a rotary evaporator at 40 °C, the solid was dissolved in *n*-hexane and filtered. The filtrate was purified by column chromatography on silica with n-hexane/ethyl acetate 9:1 as eluent (R_f = 0.34), yielding a white solid (94%, 1.1 g, 3.0 mmol).

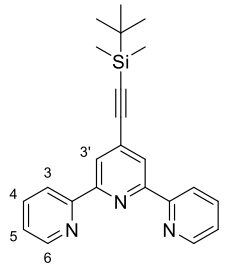

^{1}H NMR (300 MHz, chloroform-d, 298 K) δ 8.70 (ddd, *J* = 4.8, 1.8, 0.9 Hz, 1H, T6), 8.59 (dt, *J* = 8.0, 1.1 Hz, 1H, T3), 8.49 (s, 1H, T3'), 7.85 (td, *J* = 7.7, 1.8 Hz, 1H, T4), 7.34 (ddd, *J* = 7.5, 4.8, 1.2 Hz, 1H, T5), 1.01 (s, 5H), 0.21 (s, 3H). *^{13}C NMR (75 MHz, chloroform-d, 298 K)* δ 155.6 + 155.4 (T2 + T2'), 149.1 (T6), 136.9 (T4), 133.3 (T4'), 124.0 (T5), 123.2 (T3'), 121.2 (T4), 103.3 (C-C-Si), 98.03 (Ar-C-C), 26.2 (Si-C-($\underline{C}H_3)_3$), 16.7 (Si-C-$(CH_3)_3$), -4.7 (Si-($C\underline{H}_3)_2$). *ES MS m/z (calc.):* 372.5 (372.2 $[M + H]^+$).

[Ru(RCC-tpy)(Cl)$_3$] (R = TBDMS), [3]

$RuCl_3 \cdot H_2O$ (500 mg, 2.41 mmol) and RCC-tpy (895 mg, 2.41 mmol) were dissolved in ethanol (250 mL) and refluxed overnight while stirring. The reaction was cooled down to room temperature and chilled in the freezer overnight. The precipitate was filtered from the red solution and washed with cold ethanol and diethyl ether. Drying *in vacuo* yielded a brownish red solid that was used without further purification (75%, 1.05 g, 1.82 mmol).

[Ru(RCC-tpy)(bpy)(Cl)]Cl (R = TBDMS), [4]Cl

[Ru(RCC-tpy)(Cl)$_3$] (100 mg, 0.18 mmol), 2,2'-bipyridine (28 mg, 0.18 mmol), and lithium chloride (41 mg, 0.98 mmol) were dissolved in degassed ethanol/water mixture (20 mL, 3:1). Triethylamine (62 µL, 0.45 mmol) was added and the reaction mixture was stirred at 60 °C under dinitrogen atmosphere overnight. The reaction mixture was filtered hot over *Celite* and the cake was washed with ethanol. After evaporation of the combined solvents, the crude was purified by column chromatography on silica with dichloromethane/methanol (9:1, R_f = 0.42) as eluent. Evaporation of the solvent yielded [**4**]Cl as a dark purple solid (82%, 103 mg, 0.15 mmol).

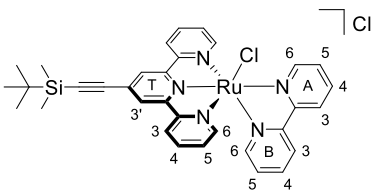

^{1}H NMR (300 MHz, methanol-d$_4$, 298 K) δ 10.19 (dd, *J* = 5.6, 1.6, 0.7 Hz, 1H, A6), 8.79 (dt, *J* = 8.2, 1.1 Hz, 1H, A3), 8.71 (s, 2H, T3'), 8.61 (dt, *J* = 8.0, 1.1 Hz, 2H, T3), 8.49 (dd, *J* = 8.1, 1.2 Hz, 1H, B3), 8.34 (td, *J* = 7.8, 1.5 Hz, 1H, A4), 8.02 (ddd, *J* = 7.4, 5.7, 1.3 Hz, 1H, A5), 7.93 (td, *J* = 7.9, 1.5 Hz, 2H, T4), 7.75 (td, *J* = 7.8, 1.4 Hz, 1H, B4), 7.69 (ddd, *J* = 5.5, 1.6, 0.8 Hz, 2H, T6), 7.43 – 7.28 (m, 3H, T5+B6), 7.05 (ddd, *J* = 7.3, 5.7, 1.4 Hz, 1H, B5), 1.12 (s, 9H, Si-C-($C\underline{H}_3)_3$), 0.32 (s, 6H, Si-($\underline{C}H_3)_2$). *^{13}C NMR (75 MHz, methanol-d$_4$, 298 K)* δ 160.1 + 157.5 (A2 + B2), 159.8 + 159.6 (T2 + T2'), 153.6 (A6), 153.2 (T6), 153.0 (B6), 138.5 (T4), 138.3 (A4), 137.1 (B4), 129.6 (T4'), 128.8 (T5), 128.2 (A5), 127.6 (B5), 125.6 (T3'), 125.3 (T3), 124.8 (A3), 124.6 (B3), 103.7+101.8 (Ar-C-C + C-C-Si), 26.6 (Si-C-($C\underline{H}_3)_3$), 17.6 (Si-C-$(CH_3)_3$), -4.6 (Si-($C\underline{H}_3)_2$). *ES MS m/z (calc.):* 664.6 (664.1, $[M - Cl]^+$).

[Ru(RCC-tpy)(bpy)(Hmte)](PF$_6$)$_2$ (R = TBDMS), [5](PF$_6$)$_2$

[Ru(RCC-tpy)(bpy)(Cl)]Cl (200 mg, 0.290 mmol) and 2-(methylthio)ethanol (1.26 mL, 14.5 mmol) were dissolved in degassed water (40 mL) and reacted at 60 °C under dinitrogen atmosphere overnight. After confirmation of reaction completion by TLC (silica, dichloromethane/methanol 9:1, R_f = 0.28), saturated aqueous potassium hexafluoridophosphate solution was added. The precipitate was filtered and rinsed carefully with ice-cold water (10 mL) and diethyl ether (25 mL). Drying *in vacuo* yielded [**5**](PF$_6$)$_2$ as an orange-brown solid (85%, 250 mg, 0.25 mmol).

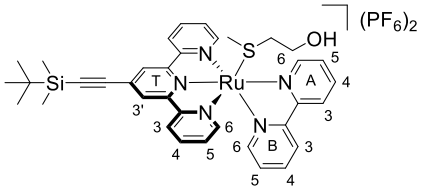

^{1}H NMR (300 MHz, acetone-d_6, 298 K) δ 9.98 (d, *J* = 5.4 Hz, 1H, A6), 8.99 (s, 2H, T3'), 8.96 (d, *J* = 8.1 Hz, 1H, A3), 8.89 (d, *J* = 8.1 Hz, 2H, T3), 8.72 (d, *J* = 8.2 Hz, 1H, B3), 8.50 (td, *J* = 7.9, 1.4 Hz, 1H, A4), 8.28 – 8.12 (m, 3H, T4 + A5), 8.09 – 7.98 (m, 3H, T6 + B4), 7.66 (dd, *J* = 6.0, 1.0 Hz, 1H, B6), 7.57 (ddd, *J* = 7.4, 5.6, 1.3 Hz, 2H, T5), 7.31 (ddd, *J* = 7.3, 5.6, 1.3 Hz, 1H, B5), 4.07 (t, *J* = 5.1 Hz, 1H, O<u>H</u>), 3.56 (dt, *J* = 5.1, 5.6 Hz, 2H, S-CH$_2$-C<u>H</u>$_2$), 2.05 – 1.99 (m, 2H, S-C<u>H</u>$_2$), 1.56 (s, 3H, S-C<u>H</u>$_3$), 1.11 (s, 9H, Si-C-(C<u>H</u>$_3$)$_3$), 0.33 (s, 6H, Si-(C<u>H</u>$_3$)$_2$). *^{13}C NMR (75 MHz, acetone-d_6, 298 K)* δ 158.7 + 158.6 (T2 + T2'), 157.7 + 157.6 (A2 + B2), 154.4 (T6), 153.1 (A6), 151.2 (B6), 139.9 (T4), 139.4 (A4), 139.3 (B4), 131.7 (T4'), 129.9 (T5), 129.0 (A5), 128.3 (B5), 127.1 (T3'), 126.4 (T3), 125.8 (A3), 124.9 (B3), 103.1 + 58.93 (Ar-<u>C</u>-C + C-<u>C</u>-Si), 59.04 (S-CH$_2$-<u>C</u>H$_2$), 37.6 (S-<u>C</u>H$_2$), 26.5 (Si-C-(<u>C</u>H$_3$)$_3$), 17.3 (Si-<u>C</u>-(CH$_3$)$_3$), 14.9 (S-<u>C</u>H$_3$), -4.6 (Si-(<u>C</u>H$_3$)$_2$). *ES MS m/z (calc.):* 360.9 (360.6, [M – 2PF$_6$]$^{2+}$).

[Ru(HCC-tpy)(bpy)(Hmte)](PF$_6$)$_2$, [2](PF$_6$)$_2$

[Ru(RCC-tpy)(bpy)(Hmte)](PF$_6$)$_2$ (250 mg, 0.247 mmol) and potassium fluoride (72 mg, 1.2 mmol) were dissolved in methanol (6 mL) and stirred at 30 °C overnight. The solvent was reduced in volume and saturated aqueous potassium hexafluoridophosphate solution was added till a precipitate was formed. The precipitate was filtered and rinsed carefully with ice-cold water (10 mL) and diethyl ether (25 mL). Drying *in vacuo* yielded **[2]**(PF$_6$)$_2$ an orange solid (76%, 168 mg, 0.187 mmol).

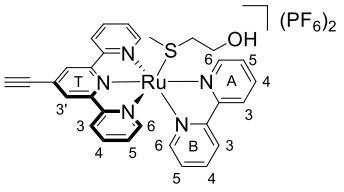

^{1}H NMR (300 MHz, acetone-d_6, 298 K) δ 9.97 (ddd, *J* = 5.6, 1.6, 0.8 Hz, 1H, A6), 8.99 (s, 2H, T3'), 8.96 (dt, *J* = 8.1, 1.1 Hz, 1H, A3), 8.88 (ddd, *J* = 7.8, 1.2, 0.6 Hz, 2H, T3), 8.72 (dt, *J* = 8.1, 1.1 Hz, 1H, B3), 8.50 (td, *J* = 7.9, 1.5 Hz, 1H, A4), 8.22 (td, *J* = 7.9, 1.5 Hz, 2H, T4), 8.19 – 8.13 (m, 1H, A5), 8.06 (ddd, *J* = 5.5, 1.5, 0.7 Hz, 2H, T6), 8.06 – 7.97 (m, 1H, B4), 7.63 (ddd, *J* = 5.7, 1.5, 0.7 Hz, 1H, B6), 7.58 (ddd, *J* = 7.7, 5.5, 1.3 Hz, 2H, T5), 7.30 (ddd, *J* = 7.2, 5.7, 1.3 Hz, 1H, B5), 4.55 (s, 1H, CC<u>H</u>), 4.06 (t, *J* = 5.1 Hz, 1H, O<u>H</u>), 3.56 (dt, *J* = 5.1, 5.7 Hz, 2H, S-CH$_2$-C<u>H</u>$_2$), 2.06 – 1.97 (m, 2H, S-C<u>H</u>$_2$), 1.56 (s, 3H, S-C<u>H</u>$_3$). *^{13}C NMR (75 MHz, acetone-d_6, 298 K)* δ 158.8 + 158.6 (T2 + T2'), 157.7 + 157.6 (A2 + B2), 154.5 (T6), 153.1 (A6), 151.2 (B6), 140.0 (T4), 139.5 (A4), 139.3 (B4), 131.3 (T4'), 129.9 (T5), 129.0 (A5), 128.3 (B5), 127.4 (T3'), 126.4 (T3), 125.8 (A3), 124.9 (B3), 87.9 (C<u>C</u>H), 81.1 (<u>C</u>CH), 59.1 (S-CH$_2$-<u>C</u>H$_2$), 37.6 (S-<u>C</u>H$_2$), 15.0 (S-<u>C</u>H$_3$). *ES MS m/z (calc.):* 303.5 (303.6, [M – 2PF$_6$]$^{2+}$). *High resolution ES MS m/z (calc.):* 303.54874 (303.54881, [M – 2PF$_6$]$^{2+}$). *Elem. Anal. Calc. for C$_{30}$H$_{27}$F$_{12}$N$_5$OP$_2$RuS:* C, 40.19; H, 3.04; N, 7.81. *Found:* C, 40.21; H, 3.06; N, 7.79.

CuAAC reaction on [2](PF$_6$)$_2$

[Ru(HCC-tpy)(bpy)(Hmte)](PF$_6$)$_2$ (41 mg, 0.046 mmol), 2-(2-(2-azidoethoxy)ethoxy)ethanol (110 mg, 0.63 mmol), CuSO$_4$·5H$_2$O (2.9 mg, 0.012 mmol), and ascorbic acid (8.4 mg, 0.042 mmol,) were added to a water/acetone mixture (9:1, 4.6 mL). The mixture was left stirring at room temperature for 1 h under air atmosphere. Acetone was removed by rotary evaporation and saturated aqueous solution of potassium hexafluoridophosphate (50 mL) was added. The product was extracted with three times with dichloromethane. After evaporation, a red-colored sticky product was obtained that was not further purified (unreacted azide still present).

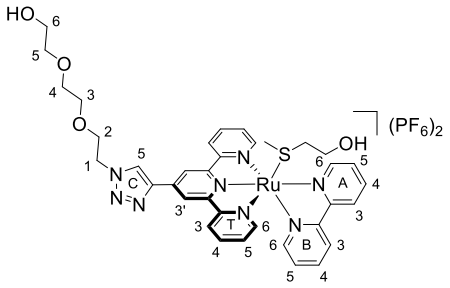

^{1}H NMR (300 MHz, acetone-d$_6$, 298 K) δ 9.95 (dd, *J* = 5.7, 1.4 Hz, 1H, A6), 9.31 (s, 2H, T3'), 9.04 (s, 1H, 5C), 9.00 – 8.86 (m, 3H, T3 + A3), 8.70 (d, *J* = 8.1 Hz, 1H, B3), 8.47 (td, *J* = 7.9, 1.5 Hz, 1H, A4), 8.20 (td, *J* = 7.9, 1.5 Hz, 2H, T4), 8.14 (ddd, *J* = 7.3, 5.6, 1.3 Hz, 1H, A5), 8.04 (d, *J* = 4.9 Hz, 2H, T6), 7.99 (dd, *J* = 7.9, 1.5 Hz, 1H, B4), 7.69 (dd, *J* = 5.7, 1.4 Hz, 1H, B6), 7.55 (ddd, *J* = 7.7, 5.5, 1.3 Hz, 2H, T5), 7.30 (ddd, *J* = 7.3, 5.7, 1.3 Hz, 1H, B5), 4.81 (t, *J* = 4.9 Hz, 2H, D1), 4.04 (t, *J* = 4.9 Hz, 2H, D2), 3.75 – 3.32 (m, D3 – D6, S-CH$_2$-CH$_2$; excess R-N$_3$), 2.01 (m, 2H, S-CH$_2$), 1.57 (s, 3H, S-CH$_3$). *^{13}C NMR (75 MHz, acetone-d$_6$, 298 K)* δ 158.9 + 158.5 (T2 + T2'), 157.7 + 157.6 (A2 + B2), 154.4 (T6), 153.0 (A6), 151.0 (B6), 144.4 (C1), 140.8 (T4'), 139.8 (T4), 139.1 (A4), 139.0 (B4), 129.6 (T5), 128.8 (A5), 128.2 (B5), 126.0 (T3), 126.0 (A3), 125.6 (C5), 124.7 (B3), 120.6 (T3'), 73.4 + 71.0 + 70.9 (D3 + D4 + D5), 69.8 (D2), 62.0 (D6), 59.0 (S-CH$_2$-CH$_2$), 51.5 (D1), 37.6 (S-CH$_2$), 14.9 (S-CH$_3$). *ES MS m/z (calc.):* 391.2 (391.1 [M − 2PF$_6$]$^{2+}$).

2.4.3 Single Crystal X-Ray crystallography

Single crystals of [**2**](PF$_6$)$_2$ were obtained by recrystallization through liquid-vapor diffusion using acetonitrile as solvent and diisopropyl ether as counter-solvent. In short, 1 mg of [**2**](PF$_6$)$_2$ was dissolved in 1 mL of acetonitrile and placed in a small vial. This vial was placed in a larger vial containing 2.8 mL diisopropyl ether. The large vial was closed, and vapor diffusion occurred within a few days to afford X-ray quality dark red rhombic crystals.

All reflection intensities were measured at 110(2) K using a SuperNova diffractometer (equipped with Atlas detector) with Cu *Kα* radiation (*λ* = 1.54178 Å) under the program CrysAlisPro (Version CrysAlisPro 1.171.39.29c, Rigaku OD, 2017). The same program was used to refine the cell dimensions and for data reduction. The structure was solved with the program SHELXS-2014/7 (Sheldrick, 2015) and was refined on F^2 with SHELXL-2014/7 (Sheldrick, 2015). Analytical numeric absorption correction using a multifaceted crystal model was applied using CrysAlisPro. The temperature of the data collection was controlled using the system Cryojet (manufactured by Oxford Instruments). The H atoms were placed at calculated positions using the instructions AFIX 23, AFIX 43, AFIX 137, AFIX 147 or AFIX 163 with isotropic displacement parameters having values 1.2 or 1.5 *U*eq of the attached C or O atoms.

The structure of [**2**](PF$_6$)$_2$ is ordered.
[**2**](PF$_6$)$_2$: 0.15 × 0.13 × 0.02 mm^3, triclinic, *P*-1, a = 9.9395 (3), b = 11.2670 (3), c = 16.2664 (4) Å, *α* = 96.662 (2), β = 91.650 (2), γ = 111.580 (2) °, V = 1677.48 (8) Å^3, Z = 2, μ = 6.21 mm^{-1}, transmission factor range: 0.485–0.882. 21777 Reflections were measured up to a resolution of (sin θ/*λ*)max = 0.616 Å^{-1}. 6568 Reflections were unique (R_{int} = 0.027), of which 6083 were observed [I > 2σ(I)]. 471 Parameters were refined. R1/wR2 [I > 2σ(I)]: 0.0273/ 0.0674. R1/wR2 [all refl.]: 0.0305/ 0.0699. S= 1.026. Residual electron density found between −0.49 and 0.90 e Å^{-3}.

2.4.4 Photochemistry

Materials

Photoreactions monitored with UV-vis were performed using a Cary 50 Varian spectrometer equipped with temperature control and a magnetic stirrer. The measurements were performed in a quartz cuvette, containing 3 mL of solution. Irradiations were carried out under air atmosphere. Irradiation was performed from the top of the cuvette perpendicularly to the optical axis of the spectrometer using a custom-build LED irradiation setup, consisting of a high-power LED driven by a LED driver operating at 350 mA.

Photoactivation

For photoactivation with green light, a LED light source (λ = 517 nm, $\Delta\lambda_{1/2}$ = 23 nm, 5.42 mW, $5.4 \cdot 10^{-8}$ mol $\cdot$ s^{-1}) was used, and absorption spectrum was measured for 70 min at T = 25 °C. [Ru] = 0.130 mM for [**1**]$(PF_6)_2$ and 0.074 mM for [**2**]$(PF_6)_2$. Data was analyzed using Microsoft Excel 2010.

Photosubstitution quantum yield

For photosubstitution quantum yield determination for [**2**]$(PF_6)_2$ (0.074 mM), a LED light source (λ = 466 nm, $\Delta\lambda 1/2$ = 36 nm, 15.4 mW, $1.11 \cdot 10^{-7}$ mol $\cdot$ s^{-1}) was used and UV-vis absorption spectra were recorded every 12 sec for 30 min at T = 37 °C. Data was analyzed using Microsoft Excel 2010. The rate constants of the photosubstitution reaction (k_Φ) was derived by fitting the time evolution of the UV-vis absorption at 450 nm to a mono-exponential decay function using Origin Pro 9.1. As the irradiation wavelength was chosen close to the isosbestic point in the photosubstitution reactions, A_{466} was assumed to be constant in time, so that the obtained rate constants could be converted into quantum yields for the photosubstitution reactions (Φ_{466}) using Equation 2.1.

$$\Phi_{466} = \frac{k_\Phi \cdot n_{Ru}}{q_p \cdot (1 - 10^{-A_{466}})} \qquad \text{Equation 2.1}$$

Here, k_Φ is the found photochemical rate constant, n_{Ru} is the total amount of ruthenium ions, q_p is the incoming photon flux, and A_{466} is the absorbance at the irradiation wavelength.

2.4.5 Mass spectrometry for Ru-BSA interaction

Sample preparation

Interactions between the photoactivable ruthenium compounds and Bovine Serum Albumin were assessed by high-resolution ESI-MS with slight modifications of the general method described in literature.[41, 50, 51] Two stock solutions of [**1**]$(PF_6)_2$ and [**2**]$(PF_6)_2$ were prepared in LC-MS grade water to a final concentration of 10^{-3} M. Another stock solution of Bovine Serum Albumin (fatty free, from Sigma-Aldrich) was prepared in LC-MS grade water at 10^{-3} M. Appropriate aliquots of these stock solutions were mixed and diluted with water to a final protein concentration of 100 μM and complex concentrations of 100, 300, or 500 μM. The reaction mixtures were prepared in duplicate for both ruthenium compounds, one sample was completely protected from light exposure and incubated up to 24 h at 37 °C. The other sample was irradiated for 1 h at 515 nm shaking at 400 rpm and then incubated for up to 24 h at 37 °C.

ESI-MS

Aliquots were sampled after 2 and 24 h and diluted with LC-MS water at 10^{-5} M protein final concentration with the addition of 0.1% formic acid. Respective ESI-MS spectra were acquired through direct infusion at 10 μL min^{-1} flow rate in a TripleTOF® 5600+ high-resolution mass spectrometer (Sciex, Framingham, MA, U.S.A.), equipped with a DuoSpray® interface operating with an ESI probe. The ESI source parameters were optimized and were as follows: positive polarity, Ionspray Voltage Floating 5400 V, Temperature 50 °C, Ion source Gas 1 (GS1) 40; Ion source Gas 2 (GS2) 0; Curtain Gas (CUR) 15, Declustering Potential (DP) 250 V, Collision Energy (CE) 10 V. For acquisition, Analyst TF software 1.7.1 (Sciex) was used and deconvoluted spectra were obtained by using the Bio Tool Kit micro-application v.2.2 embedded in PeakView™ software v.2.2 (Sciex).

ICP-AES

The residual fractions of the reaction mixtures prepared for the MS analysis (about 0.9 mL) were used for the ICP-AES determination of the ruthenium bound to the protein, following a well-established protocol.[52, 53] The metallated proteins were isolated using a centrifugal filter device with a cut-off membrane of 10 kDa and washed several times with LC-MS grade water. The final metal/protein adducts were recovered by spinning the filters upside-down at 3500 rpm for 3 min with 200 μL of water. The samples were mineralized in a thermoreactor at 90 °C for 8 h with 1.0 mL of HCl 30% Suprapur grade (Merck Millipore). After that, the samples were diluted exactly to 6.0 mL with MilliQ water (≤18 MΩ). The determination of ruthenium content in these solutions was performed using a Varian 720-ES Inductively Coupled Plasma Atomic Emission Spectrometer (ICP-AES). The calibration curve of ruthenium was obtained using known concentrations of a Ru ICP standard solution purchased from Sigma-Aldrich. Moreover, each sample was spiked with 1 ppm of Ge used as an internal standard. The wavelength used for Ru determination was 267.876 nm whereas for Ge the line at 209.426 nm was used. The operating conditions were optimized to obtain maximum signal intensity and, between each sample, a rinse solution containing 1.0 mL of HCl 30% Suprapur grade and 5.0 mL of ultrapure water was used to avoid any "memory effect".

2.4.6 Fluorophore labeling

Materials

BSA and tris(3-hydroxypropyltriazolylmethyl)amine were purchased from Sigma Aldrich, Alexa Fluor™ 647 azide as triethylammonium salt from Thermo Fisher.

Click reaction

BSA (in 1X PBS, 15 μM) was incubated with **[2]**$(PF_6)_2$ (in DMSO, 75 μM) at 37 °C in the dark for 24 h under constant shaking. After activation with green light (520 nm, 76 J · cm^2) for 1 h, the solution was incubated at 37 °C in the dark for an additional 24 h. Samples (50 μL) were taken before and after light activation (6 and 24 h after activation). Dark control samples as well as negative controls (without complex, without BSA or without fluorophore) which were not activated were collected at the same time points. Samples were stored at -20 °C if not used directly. For the click reaction, each sample was incubated with an equivalent amount of click cocktail (50 μL, copper sulfate (6.4 mM), sodium ascorbate (37.5 mM), tris(3-hydroxypropyltriazolylmethyl)amine (THPTA) (in DMSO, 1.3 mM), Tris-HCl (100 mM, pH 8.0), and Alexa Fluor 647 azide (in DMSO, 5 μM)) at r.t under gentle shaking for 1 h in the dark. The click reaction was quenched with SDS loading Buffer (50 μL) and used immediately for in-gel fluorescence.

Alkyne-substituted vinculin, Homopropargylglycine-Vin (Hpg-Vin), was used as positive control and prepared by Dr. Can Araman according to a published procedure.[54]

Note that electrophoresis was performed in the dark. 2 μg of protein was added to each well of a 15 well 1.5 mm SDS gel at 200 V for 1 h. Protein concentration of each sample was measured using a Qubit reader (Thermo Fisher). Fluorescent bands of the SDS gels were visualized using a BioRad ChemiDoc™ Touch Imaging System with Alexa647 filter. Coomassie staining was applied overnight and de-stained with the destaining solution (MeOH:water:AcOH; 5:4:1).

2.4.7 Supporting Information

^{1}H NMR spectra of [**5**](PF$_6$)$_2$, [**2**](PF$_6$)$_2$, and the click product, dark stability measurements, singlet oxygen production and phosphorescence spectra, UV-vis spectra of BSA interaction, and images of SDS PAGE gel electrophoresis are provided in Appendix AII.

2.5 Contribution

Dr. Can Araman supervised the Ru-BSA interaction SDS gel experiments performed by Ingrid Flashpohler. Dr. Alessandro Pratesi and Prof. Luigi Messori performed ESI MS measurements. Dr. Vincent van Rixel grew single crystals, and Dr. Maxime Siegler performed X-ray diffraction experiments and crystal structure determination. Dr. Sylvestre Bonnet, Dr. Can Araman, and Prof. Lies Bouwman provided experimental guidance and significant editorial feedback.

2.6 References

1 M. Groessl, O. Zava, and P. J. Dyson, *Metallomics* **2011**, 3 (6), 591-599.

2 A. Frei, R. Rubbiani, S. Tubafard, O. Blacque, P. Anstaett, A. Felgenträger, T. Maisch, L. Spiccia, and G. Gasser, *J. Med. Chem.* **2014**, 57 (17), 7280-7292.

3 T. S. Morais, F. C. Santos, T. F. Jorge, L. Côrte-Real, P. J. A. Madeira, F. Marques, M. P. Robalo, A. Matos, I. Santos, and M. H. Garcia, *J. Inorg. Biochem.* **2014**, 130 1-14.

4 L. Côrte-Real, F. Mendes, J. Coimbra, T. S. Morais, A. I. Tomaz, A. Valente, M. H. Garcia, I. Santos, M. Bicho, and F. Marques, *J. Biol. Inorg. Chem.* **2014**, 19 (6), 853-867.

5 Walker Henry K, Hall Wilbur D, and H. J. W, Clinical Methods: The History, Physical, and Laboratory Examinations. **1990,** 3rd.

6 M. P. Sullivan, H. U. Holtkamp, and C. G. Hartinger, Antitumor Metallodrugs that Target Proteins in *Metallo-Drugs: Development and Action of Anticancer Agents* **2018**, 351-386.

7 Y. Zhang, A. Ho, J. Yue, L. Kong, Z. Zhou, X. Wu, F. Yang, and H. Liang, *Eur. J. Med. Chem.* **2014**, 86 449-455.

8 J. Mayr, P. Heffeter, D. Groza, L. Galvez, G. Koellensperger, A. Roller, B. Alte, M. Haider, W. Berger, C. R. Kowol, and B. K. Keppler, *Chem. Sci.* **2017**, 8 (3), 2241-2250.

9 A. Bergamo, A. Masi, A. F. A. Peacock, A. Habtemariam, P. J. Sadler, and G. Sava, *J. Inorg. Biochem.* **2010**, 104 (1), 79-86.

10 A. R. Timerbaev, C. G. Hartinger, S. S. Aleksenko, and B. K. Keppler, *Chem. Rev.* **2006**, 106 (6), 2224-2248.

11 G. Ferraro, L. Massai, L. Messori, and A. Merlino, *Chem. Commun.* **2015**, 51 (46), 9436-9439.

12 A. Wragg, M. R. Gill, L. McKenzie, C. Glover, R. Mowll, J. A. Weinstein, X. Su, C. Smythe, and J. A. Thomas, *Chem. Eur. J.* **2015**, 21 (33), 11865-11871.
13 B. X. Huang, H.-Y. Kim, and C. Dass, *J. Am. Soc. Mass Spectrom.* **2004**, 15 (8), 1237-1247.
14 A. Bijelic, S. Theiner, B. K. Keppler, and A. Rompel, *J. Med. Chem.* **2016**, 59 (12), 5894-5903.
15 A. Merlino, *Coord. Chem. Rev.* **2016**, 326 111-134.
16 A. Casini, A. Karotki, C. Gabbiani, F. Rugi, M. Vasak, L. Messori, and P. J. Dyson, *Metallomics* **2009**, 1 (5), 434-441.
17 F. Piccioli, S. Sabatini, L. Messori, P. Orioli, C. G. Hartinger, and B. K. Keppler, *J. Inorg. Biochem.* **2004**, 98 (6), 1135-1142.
18 L. Trynda-Lemiesz, A. Karaczyn, B. K. Keppler, and H. Kozlowski, *J. Inorg. Biochem.* **2000**, 78 (4), 341-346.
19 J. D. White, M. F. Osborn, A. D. Moghaddam, L. E. Guzman, M. M. Haley, and V. J. DeRose, *J. Am. Chem. Soc.* **2013**, 135 (32), 11680-11683.
20 S. Ding, X. Qiao, J. Suryadi, G. S. Marrs, G. L. Kucera, and U. Bierbach, *Angew. Chem.* **2013**, 125 (12), 3434-3438.
21 H. C. Kolb, M. G. Finn, and K. B. Sharpless, *Angew. Chem., Int. Ed.* **2001**, 40 (11), 2004-2021.
22 V. V. Rostovtsev, L. G. Green, V. V. Fokin, and K. B. Sharpless, *Angew. Chem., Int. Ed.* **2002**, 41 (14), 2596-2599.
23 A. Baron, C. Herrero, A. Quaranta, M.-F. Charlot, W. Leibl, B. Vauzeilles, and A. Aukauloo, *Inorg. Chem.* **2012**, 51 (11), 5985-5987.
24 K. P. Chitre, E. Guillén, A. S. Yoon, and E. Galoppini, *Eur. J. Inorg. Chem.* **2012**, 2012 (33), 5461-5464.
25 I. Ott, K. Schmidt, B. Kircher, P. Schumacher, T. Wiglenda, and R. Gust, *J. Med. Chem.* **2005**, 48 (2), 622-629.
26 N. Zabarska, D. Sorsche, F. W. Heinemann, S. Glump, and S. Rau, *Eur. J. Inorg. Chem.* **2015**, 2015 (29), 4869-4877.
27 J. B. Gerken, M. L. Rigsby, R. E. Ruther, R. J. Pérez-Rodríguez, I. A. Guzei, R. J. Hamers, and S. S. Stahl, *Inorg. Chem.* **2013**, 52 (6), 2796-2798.
28 H. T. Ratte, *Environ. Toxicol. Chem.* **1999**, 18 (1), 89-108.
29 A. Bahreman, B. Limburg, M. A. Siegler, E. Bouwman, and S. Bonnet, *Inorg. Chem.* **2013**, 52 (16), 9456-69.
30 N. J. Farrer, L. Salassa, and P. J. Sadler, *Dalton Trans.* **2009**, - (48), 10690-10701.
31 S. Bonnet, *Dalton Trans.* **2018**, 47 (31), 10330-10343.
32 R. E. Goldbach, I. Rodriguez-Garcia, J. H. van Lenthe, M. A. Siegler, and S. Bonnet, *Chem.Eur. J.* **2011**, 17 (36), 9924-9929.
33 J. Rodríguez, J. Mosquera, J. R. Couceiro, M. E. Vázquez, and J. L. Mascareñas, *Angew. Chem.* **2016**, 128 (50), 15844-15847.
34 C. Scolaro, C. G. Hartinger, C. S. Allardyce, B. K. Keppler, and P. J. Dyson, *J. Inorg. Biochem.* **2008**, 102 (9), 1743-1748.
35 P. G. M. Wuts and T. W. Greene, Protection for the Alkyne-CH in *Greene's Protective Groups in Organic Synthesis* **2007**, 927-933.
36 R. Ziessel, V. Grosshenny, M. Hissler, and C. Stroh, *Inorg. Chem.* **2004**, 43 (14), 4262-4271.
37 C. Ruppin and P. H. Dixneuf, *Tetrahedron Lett.* **1986**, 27 (52), 6323-6324.
38 V. H. S. van Rixel, G. F. Moolenaar, M. A. Siegler, L. Messori, and S. Bonnet, *Dalton Trans.* **2018**, 47 (2), 507-516.

39 A. Casini, G. Mastrobuoni, W. H. Ang, C. Gabbiani, G. Pieraccini, G. Moneti, P. J. Dyson, and L. Messori, *ChemMedChem* **2007**, 2 (5), 631-635.

40 C. G. Hartinger, M. Groessl, S. M. Meier, A. Casini, and P. J. Dyson, *Chem. Soc. Rev.* **2013**, 42 (14), 6186-6199.

41 E. Michelucci, G. Pieraccini, G. Moneti, C. Gabbiani, A. Pratesi, and L. Messori, *Talanta* **2017**, 167 30-38.

42 J. R. Brown, Serum Albumin: Amino Acid Sequence in *Albumin: Structure, Function and Uses* **1977**, 27-52.

43 F. Wang, H. Chen, J. A. Parkinson, P. d. S. Murdoch, and P. J. Sadler, *Inorg. Chem.* **2002**, 41 (17), 4509-4523.

44 D. Lazić, A. Arsenijević, R. Puchta, Ž. D. Bugarčić, and A. Rilak, *Dalton Trans.* **2016**, 45 (11), 4633-4646.

45 F. Wang, J. Bella, J. A. Parkinson, and P. J. Sadler, *J. Biol. Inorg. Chem.* **2005**, 10 (2), 147-155.

46 G. J. Quinlan, G. S. Martin, and T. W. Evans, *Hepatology* **2005**, 41 (6), 1211-1219.

47 V. H. S. van Rixel, A. Busemann, A. J. Göttle, and S. Bonnet, *J. Inorg. Biochem.* **2015**, 150 174-181.

48 M. I. Webb, R. A. Chard, Y. M. Al-Jobory, M. R. Jones, E. W. Y. Wong, and C. J. Walsby, *Inorg. Chem.* **2012**, 51 (2), 954-966.

49 Y.-R. Zheng, K. Suntharalingam, T. C. Johnstone, H. Yoo, W. Lin, J. G. Brooks, and S. J. Lippard, *J. Am. Chem. Soc.* **2014**, 136 (24), 8790-8798.

50 T. Marzo, S. A. De Pascali, C. Gabbiani, F. P. Fanizzi, L. Messori, and A. Pratesi, *BioMetals* **2017**, 30 (4), 609-614.

51 A. Pratesi, D. Cirri, L. Ciofi, and L. Messori, *Inorg. Chem.* **2018**, 57 (17), 10507-10510.

52 I. Landini, A. Lapucci, A. Pratesi, L. Massai, C. Napoli, G. Perrone, P. Pinzani, L. Messori, E. Mini, and S. Nobili, *Oncotarget* **2017**, 8 (56), 96062-96078.

53 S. Ciambellotti, A. Pratesi, M. Severi, G. Ferraro, E. Alessio, A. Merlino, and L. Messori, *Dalton Trans.* **2018**, 47 (33), 11429-11437.

54 C. M. C. Araman, L. Pieper-Pournara, A. S. B. Kampstra, M. H. S. Marqvorsen, C. Nascimento, W. van der Wulp, M. G. J. M. Groenewold, M. G. M. Camps, F. Ossendorp, R. Toes, and S. I. van Kasteren, *bioRxiv* **2018**, 439323.